www.amlett.com, www.vbripress.com/aml, DOI: 10.5185/amlett.2015.6017 Published online by the VBRI Press in 2015

Correlation between oxygen partial pressure and properties of pulsed laser deposited SnO_2/Fe_2O_3 composite films

M. Chowdhury[1], S.K. Sharma[1*], R.J. Chaudhary[2]

[1]*Department of Applied Physics, Indian School of Mines, Dhanbad 826004, India*
[2]*UGC-DAE Consortiums for Scientific Research, Khandwa Road, Indore 452017, India*

[*]Corresponding author. Tel: (+91) 3262235412; E-mail: sksharma.ism@gmail.com

Received: 10 June 2015, Revised: 07 August 2015 and Accepted: 04 September 2015

ABSTRACT

SnO_2/Fe_2O_3 composite thin films were deposited on quartz substrates at various oxygen partial pressures with a substrate temperature of 750 °C by pulsed laser deposition. The structural and optical properties of the deposited films were studied by X-ray diffraction (XRD), Atomic force microscopy (AFM), UV–visible spectroscopy and Photoluminescence. X-ray diffraction analysis revealed the formation of mixed phases (tetragonal SnO_2 and hexagonal α-Fe_2O_3) at lower oxygen partial pressure (0.1 mTorr) and only tetragonal phase at higher oxygen partial pressures (50-250 mTorr). Atomic force microscopy studies show the dense and uniform distribution of composite films. The average RMS roughness of the films increases with increasing oxygen partial pressure. The bandgap was found varying between 3.55 and 3.85 eV for different oxygen pressures. A strong broad blue emission band was observed for all the oxygen partial pressures. The origin of the blue emission in the composite film is discussed with the help of vacancy creation. A correlation between oxygen partial pressure and the properties of SnO_2/Fe_2O_3 composite films is suggested. Copyright © 2015 VBRI Press.

Keywords: Thin film; X-ray diffraction; photoluminescence.

Introduction

Metal oxide semiconductors have attracted a wide interest due to their potential applications in gas sensor [**1-3**], lithium-ion battery [**4**] and catalysis [**5, 6**]. Metal oxides have tunable properties and important technological applications. Among them, SnO_2 as an important n-type semiconductor with bandgap of~ 3.6 eV have been intensively investigated as optoelectronic devices, gas sensors, photocatalysts and electrodes [**7**]. In a similar manner, Fe_2O_3 an n-type semiconductor with a bandgap of~ 2.2 eV is a promising material as a gas sensor, photoelectrode and catalysts [**8, 9**]. Recent studies confirm that the performance of SnO_2 or Fe_2O_3 can be significantly improved by formation of SnO_2/Fe_2O_3 composites [**5, 10**]. To modify the conductivity, optical absorption and gas sensitivity, incorporation of certain additives, mostly of transition metal oxides are required [**11, 12**]. Doping indicates the addition of small quantity. But in composite materials, a high level of doping was done which disorders the host system and the resistive properties were modified which can be applied in TCOs.

In recent years, efforts have been made to synthesize SnO_2/Fe_2O_3 composites using sol–gel [**13**], hydrothermal [**14**] and chemical vapor deposition [**15**]. Literature survey reveals that there is no report on the correlation between oxygen partial pressure and the properties of SnO_2/Fe_2O_3 composite films synthesized by pulsed laser deposition (PLD). PLD is known technique for the synthesis of oxide thin films because of its advantages in the stoichiometry conservation, reduced contamination due to the use of laser light and control of the composition of deposited structure. It is also a versatile technique for the production of desired size and composition of nanoparticles by varying the deposition parameters [**16**]. The concentration of oxygen in PLD technique plays a vital role. Due to lack of oxygen atoms, residual stress formed in the film leads to cracking of the films which causes optical degradation. In case of excessive oxygen, the grain boundary oxygen atoms trap free electrons which absorb radiation in the infrared region [**17**].

Optoelectronic properties of SnO_2 or Fe_2O_3 depend on the presence of impurities and its stoichiometry with respect to oxygen. Photoluminescence (PL) studies provide crucial information about the structure, defects and impurities in a material. Bulk SnO_2 crystals show very low emission efficiency at room temperature. Several researchers have reported the PL properties of SnO_2 nanostructures [**18, 19**]. SnO_2 shows PL at near band edge (NBE) and deep level emission (DLE) under the excitation of 325 nm radiation at room temperature. The PL in SnO_2 originates mainly due to the presence of energy states in the band gap associated with the defects like tin interstitials (Sn_i), dangling bonds and oxygen vacancies (V_o) [**19**]. It is

recognized that oxygen vacancies play an important role in the luminescence bands of SnO_2. Here, in the present studies, the occurrence of blue emission is explained with the help of oxygen vacancies.

In the present investigation, SnO_2/Fe_2O_3 composite films were synthesized by PLD technique and their structural and optical properties were studied as a function of oxygen partial pressure. The aim of the present work was to establish a correlation between the oxygen partial pressure and the properties of SnO_2/Fe_2O_3 composite films.

Experimental

Material synthesis

Powder blends of SnO_2 and Fe_2O_3 containing 50 wt% SnO_2 and 50 wt% Fe_2O_3 were properly weighed, mixed and thoroughly ground in a mortar by mechanical means to produce homogeneous distribution. These powder blends were subsequently used to produce 1 inch diameter pellets through cold pressing by applying 6 ton load. The prepared pellets were sintered in air at 1100°C for 4 hours. KrF excimer laser (Lambda Physik COMPEX, λ = 248 nm and pulsed duration of 25 ns) was used to deposit SnO_2 /Fe_2O_3 composite thin films. The laser was operated at a pulse rate of 10 Hz and energy of 210 mJ. Thin films were deposited under oxygen partial pressures of 0.1 mT, 50 mT and 250 mT. All the films were grown at substrate temperature of 750 °C. A quartz substrate was first cleaned by acetone followed by methanol for 5 min in ultrasonic cleaner and then mounted on a substrate holder inside the deposition chamber and placed parallel to the target at a perpendicular distance of 45 mm. The deposition chamber was initially evacuated to 2.0 x 10^{-6} Torr and oxygen gas was introduced into the chamber during deposition to obtain the above pressures.

Characterizations

The structural properties of the SnO_2-Fe_2O_3 composites were recorded in a wide range of Bragg angle 2θ (20° ≤ 2θ ≤ 80°) with a 0.03° sampling pitch using Bruker D8 Advance X-ray diffractometer with CuK_α radiation (λ = 0.1542 nm). Atomic force microscopy (AFM) (Digital Instruments Nanoscope-IV, with Si_3N_4 100 μm cantilever, 0.56 N/m force constant) studies were performed to observe the surface morphology in contact mode. The optical transmission spectra were recorded by Perkin-Elmer Lambda 35 spectrophotometer in the wavelength range of 190-1100 nm. The photoluminescence studies were carried out on Hitachi make Fluorescence Spectrometer F-2500 in the wavelength range 220 - 800 nm. The electrical properties of the deposited thin films were measured by four probe arrangement at room temperature.

Results and discussion

X-ray diffraction (XRD)

Fig. 1 shows the XRD patterns of SnO_2/Fe_2O_3 composite thin films deposited at different oxygen partial pressures. The diffraction peaks around 2θ at 33.7°, 37.8°, 51.6°and 54.5° indicate the formation of tetragonal SnO_2 phase and the peak at around 36.2° indicate the hexagonal α-Fe_2O_3 phase. The film deposited at 0.1 mTorr oxygen partial pressure is polycrystalline in nature. The intensity of (200) diffraction peak increases with the increase of oxygen pressure from 0.1 mTorr to 50 mTorr and then decreases for the film deposited at 250 mTorr oxygen pressure. This is attributed to the reduction of the adhesion coefficient for the target element which arrives at the substrate. The degradation of the crystalline quality beyond an optimal oxygen pressure is due to the induced defects by excess of oxygen which interfere with the nucleation and growth of the films [**20**]. In addition, the grown film at 0.1 mTorr has high orientation in the plane (110), but at higher pressures the plane (200) increases evidently, indicating the crystal reorientation effect. It can be explained on the basis of the crystallographic orientation explained by Korber *et al.* [**21**]. A transition from reduced to oxidized surface termination and the related surface energy stability are the main cause for this crystallographic orientation.

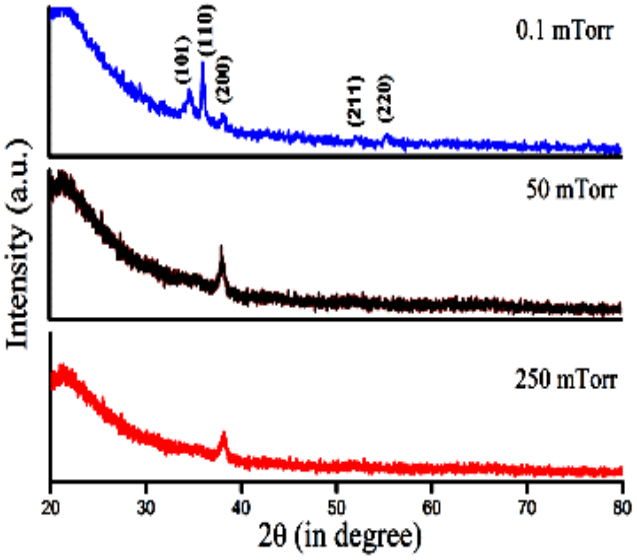

Fig. 1. XRD patterns of composite films at different oxygen pressure.

Crystallite size

The crystallite size of the composite films was calculated using Debye–Scherrer's equation [**22**].

$$D = \frac{k\lambda}{\beta \cos\theta} \quad (1)$$

where, k is the correlation factor (0.94), β is the full width at half-maximum (FWHM) of the most intense diffraction peak, λ is the wavelength of the Cu Kα radiation and θ is the Bragg angle. The Full Width at Half Maximum (FWHM) and crystallite size of composite films grown at various oxygen pressures are shown in **Table 1**. The decrease of FWHM with increase of oxygen pressure indicates an increase in crystallite size of composite films. This increase in crystallite size (**Fig. 2**) is due to the interaction and agglomeration of crystallites with each other at high oxygen pressure [**20**].

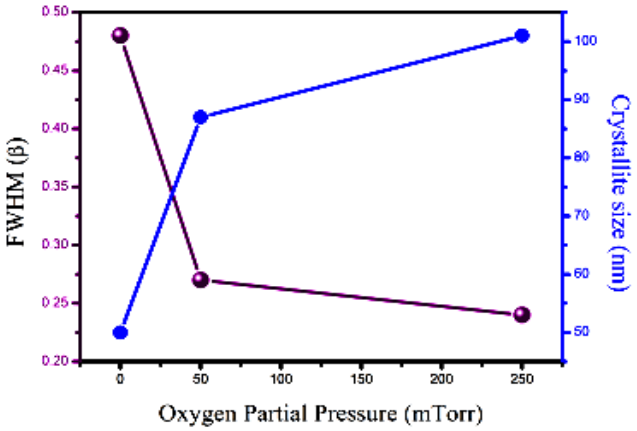

Fig. 2. Variation of FWHM and crystallite size as a function of oxygen pressure.

Atomic force microscopy (AFM)

Fig. 3 shows the 3D AFM images of composite films deposited on quartz substrates at different oxygen partial pressures. The AFM images show that the films contain uniform distribution of crystallites with dense structure. The atoms form a fairly smooth surface due to high kinetic energy and mobility at low oxygen pressure.

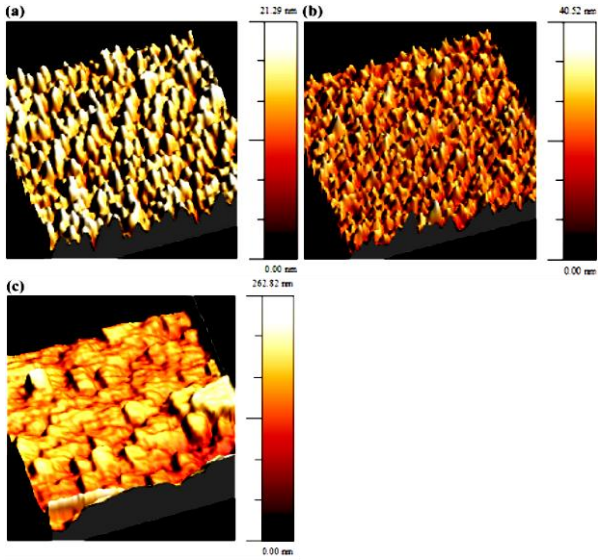

Fig. 3. AFM images of composite films at (a) 0.1, (b) 50 and (c) 250 mTorr.

At higher oxygen pressure, the surface roughness increases which is attributed to the scattering of ablated species with the oxygen molecules which decreases the energy of atoms and hence decreases the capability of atoms to move on the substrate surface [**23**]. The values of average RMS surface roughness are shown in **Table 1**.

Table 1. Structural parameters of composite films at different oxygen pressure.

Oxygen pressure (mTorr)	Full Width at Half Maxima (degree)	Crystallite size (nm)	Surface roughness (nm)
0.1	0.48	50	2.1
50	0.27	87	3.9
250	0.24	101	15.6

Transmission spectra

The optical transmission spectra of composite films deposited at different oxygen pressures are shown in **Fig. 4(a)**. It shows that the optical properties vary systematically with changing oxygen partial pressure. The improvement of optical transmission with increase oxygen partial pressure can be attributed to the increase of grain size resulting an increase in absorption of light [**20**]. However, at higher oxygen partial pressures the transmittance decreased due to reducing of adatoms mobility. The rough surfaces may cause the low optical transmittance due to scattering loss and this high surface roughness was also evident from AFM studies.

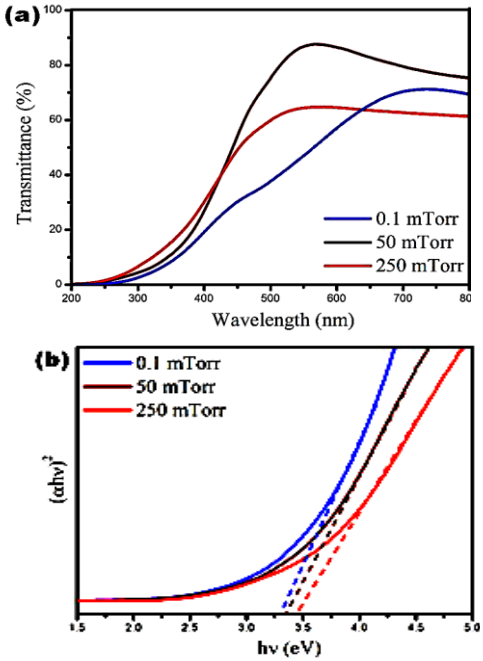

Fig. 4. (a) Transmission spectra (b) Plot of $(\alpha h\nu)^2$ versus hν of composite films at different oxygen pressure.

Bandgap

The absorption coefficient and optical band gap of the deposited films were calculated from the transmission spectra using the following relations [**24**],

$$\alpha = \frac{1}{d}\ln\left(\frac{1}{T}\right) \quad (2)$$

$$\alpha h\nu = A(h\nu - E_g)^n \quad (3)$$

where, T is the transmittance and d is the film thickness. A is a constant, h is the Planck's constant, n is the frequency of radiation which depends on the kind of optical transitions and E_g is the optical band gap. From the plot of $(\alpha h\nu)^2$ vs hν (**Fig. 4(b)**), the bandgap values were obtained by extrapolating the straight line portion of $(\alpha h\nu)^2$ versus hν plot to hν = 0 for all the deposited films according to equation (3). The bandgap values are listed in **Table 2**. As the oxygen pressure increases from 0.1 to 50 mTorr, the bandgap increases. The increment of band gap with oxygen partial pressure is due to the decrease of oxygen vacancies in the composite films. Since smaller vacancies offer

smaller defect states near the conduction band edge, which effectively leads to increase the band. The content of oxygen vacancies decreases with oxygen partial pressure and hence carrier concentration decreases. So the band gap increases with increase of oxygen partial pressure [**20**].

Photoluminescence (PL)

Fig. 5(a) shows the photoluminescence emission spectra for composite films deposited at different oxygen partial pressure. The PL intensity increases with the increase in oxygen pressure. Here we have deconvoluted the PL spectra to understand the origin of the emission peaks using Gaussian fitting.

The inset of **Fig. 5(a)** represents one of the deconvoluted spectra for the film deposited at 250 mTorr. Here the peak positions in the spectra helped us to locate the energy levels associated with the intrinsic defects. It is quite evident from **Fig. 5(a)** that the positioning of the emission bands are lower than the respective band gap of the SnO_2 which suggests that the emission cannot be assigned to the direct recombination of a conduction electron in the Sn 4p band and a hole in the O 2p valence band. The different luminescent centres such as various defects and dangling bonds in the films [**25**] are responsible for the broad emissions in the spectra. H. Sefardjella *et al.* [**19**] observed PL spectra of SnO_2 peaking at 396 and 439 nm. Here, the PL spectra shift towards higher wavelength mainly peaking at ~ 446 nm. This was mainly due to the addition of Fe_2O_3. Generally, in oxides, oxygen vacancy is known to be the most common defect and usually acts as the radiative centre by forming the defect levels located inside the band gap and trapping electrons from the valence band. The oxygen vacancies are mostly found to be present in three different charge states in the oxides such as neutral oxygen vacancies (V_o), singly occupied oxygen vacancies ($V_o^{\bullet}$) and doubly occupied oxygen vacancies ($V_o^{\bullet\bullet}$) [**26**]. There are many $V_o^{\bullet}$ in SnO_2 and these are assumed to be the recombination centres for the luminescence process. In addition, the visible broad emission around 400-500 nm is attributed to the formation of a $V_o^{\bullet\bullet}$ luminescent centre. The increase in oxygen partial pressure increases the concentration of oxygen vacancies resulting an increase in PL intensity.

CIE parameters

The CIE parameters such as colour coordinate (x, y) and colour correlated temperature (CCT) were calculated in order to know the photometric characteristics of the prepared composite films. The Colour coordinates (x, y) were calculated by the spectrophotometric method using the spectral energy distribution of the emission spectra [**27**]. The colour correlated temperatures were calculated by the McCamy empirical formula [**28**]:

$$CCT = -473n^3 + 3601n^2 - 6861n + 5514.31 \quad (4)$$

where, n = $(x-x_e) / (y-y_e)$ is the inverse slope line, and the CCT epicentre is $x_e = 0.3320$ and $y_e = 0.1858$.

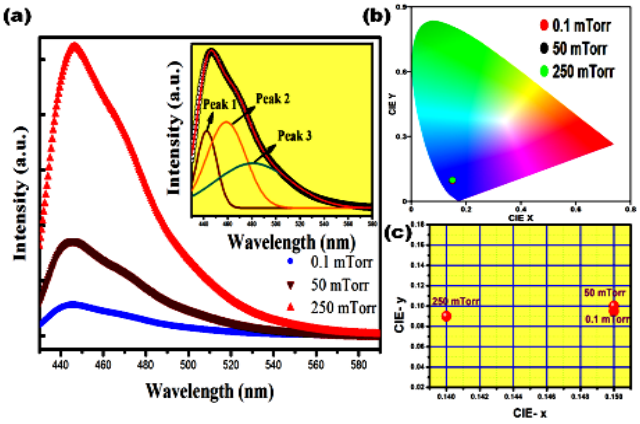

Fig. 5. (a) Photoluminescence spectra (b-c) CIE diagram of composite films at different oxygen pressure.

The calculated CIE parameters under different oxygen pressures are given in **Table 2**. The colour coordinates are marked in CIE chromaticity diagram (**Fig. 5(b)**). **Fig. 5(c)** shows clearly the invariance of colour coordinate with oxygen pressure. No variation in the position of colour coordinates with oxygen pressure was observed indicating the stability of the colour. CCT values well below 5000 K were obtained.

Resistivity measurement

The variation of electrical resistivity of SnO_2-Fe_2O_3 composite thin films as a function of oxygen partial pressure is shown in **Fig. 6**.

Table 2. Optical parameters of composite films at different oxygen pressure.

Oxygen pressure (mTorr)	Bandgap (eV)	Colour Coordinate		Color Correlated Temperature (K)
		x	y	
0.1	3.30	0.15	0.095	2710
50	3.36	0.15	0.10	2992
250	3.44	0.14	0.09	2709

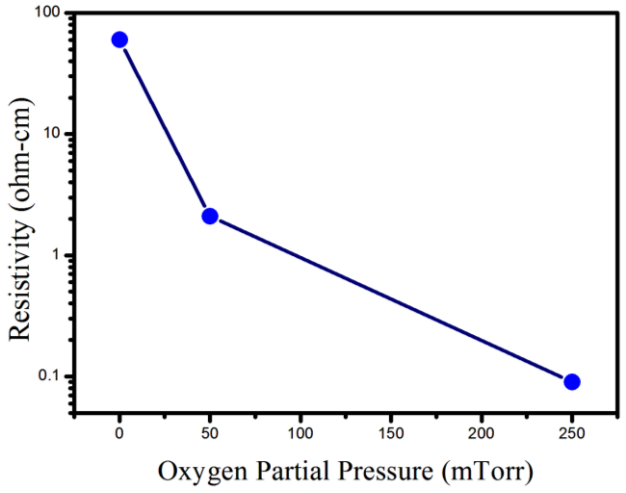

Fig. 6. Variation of resistivity of composite films as a function of oxygen pressure.

The increasing grain size leads to the decrease in the resistivity with oxygen partial pressure. The decrease in the resistivity can be attributed to the lower grain boundary scattering due to the larger grain size [**29**]. A comparison of the present work with the existing literature is summarized in **Table 3**.

Table 3. Comparison with existing literature.

Sample Name	Preparation method	Resistivity (Ω-cm)	Reference
SnO_2:Sb	DC Magnetron Sputtering	~10^{-3}	**[30]**
SnO_2	Thermal evaporation	-	**[31]**
SnO_2	Thermal evaporation	~10^{-1}	**[32]**
SnO_2:Te	Pulsed Laser Deposition	~10^{-2}	**[33]**
SnO_2-Fe_2O_3	Pulsed Laser Deposition	~10^{-2}	**Present Work**

Conclusion

The structural and optical properties were investigated for the optimization of the deposition parameters of SnO_2/Fe_2O_3 composite thin films. XRD analysis indicates that the preferential orientation is related to the variation of the oxygen partial pressure. The AFM images show the dense and uniform distribution of the films. The crystallite size and average surface roughness of the films increase with increasing oxygen pressure. The increase in crystallite size favors the improvement in the optical transmittance and band gap. These properties are sensitive to the variation in oxygen partial pressure which is suitable for sensor applications. It can also be useful in the development of tunable source or detectors in UV-range. The stability of strong blue emission band against the oxygen partial pressure and the values of colour correlated temperature well below 5000 K indicate the application of deposited films in display devices. The minimum resistivity of the composite films is obtained for 250 mTorr oxygen partial pressure.

Acknowledgments
The authors would like to thank Dr. Mukul Gupta and Dr.V. Ganesan, UGC-DAE CSR Indore for XRD and AFM studies.

Reference

1. Chu, D. W.; Zeng, Y. P.; Jiang, D. L.; Masuda, Y.; *Sens. Actuators, B: Chem.*, **2009**, *137*, 630. **DOI:** 10.1016/j.snb.2008.12.063
2. Enachi, M.; Lupan, O.; Braniste, T.; Sarua, A.; Chow, L.; Mishra, Y. K.; Gedamu, D.; Adelung, R.; Tiginyanu, I.; *Phys. Status Solidi*, **2015**, *9*, 171. **DOI:** 10.1002/pssr.201409562
3. Lupan, O.; Braniste, T.; Deng, M.; Ghimpu, L.; Paulowicz, I.; Mishra, Y. K.; Kienle, L.; Adelung, R.; Tiginyanu, I.; *Sens. Actuators B: Chemical*, **2015**, *221*, 544. **DOI:** 10.1016/j.snb.2015.06.112
4. Niu, M. T.; Huang, F.; Cui, L. F.; Huang, P.; Yu, Y. L.; Wang, Y. S.; *ACS Nano*, **2010**, *4*, 681. **DOI:** 10.1021/nn901119a
5. Zhou, W.; Cheng, C.; Liu, J.; Tay, Y. Y.; Jiang, J.; Jia, X.; Zhang J.; Gong, H.; Hng, H. H.; Yu, T.; Fan, H. J.; *Adv. Funct. Mater.*, **2011**, *21*, 2439. **DOI:** 10.1002/adfm.201100088
6. Mishra, Y. K.; Modi, G.; Cretu, V.; Postica, V.; Lupan, O.; Reimer, T.; Paulowicz, I.; Hrkac, V.; Benecke, W.; Kienle, L.; Adelung, R.; *ACS Appl. Mater. Interfaces*, **2015**, *7*, 14303. **DOI:** 10.1021/acsami.5b02816
7. Batzill, M.; Diebold, U.; *Prog. Surf. Sci.*, **2005**, *79*, 47. **DOI:** 10.1016/j.progsurf.2005.09.002
8. Huo, L.; Li, W; Lu, L; Cai, H; Xi, S; Wang, J; Zhao, B; Shen, Y.; Lu, Z.; *Chem. Mater.*, **2000**, *12*, 790. **DOI:** 10.1021/cm990690+
9. Kung, H. H.; Transition Metal Oxides: Surface Chemistry and Catalysis; Elsevier: New York, **1989**.
10. Wu, W; Zhang, S. F.; Ren, F.; Xiao, X. H.; Zhou, J.; Jiang, C. Z.; *Nanoscale*, **2011**, *3*, 4676. **DOI:** 10.1039/c1nr10728c
11. Tiwary, M.; Singh, K.; Subramanian, A.; Agarwal, D. C.; Avasthi, D. K.; Mishra, Y. K.; Mazzoldi, P.; Mattei, G.; Sada, C.; Trave, E.; Battaglin, G.; *Vacuum*, **2011**, *85*, 806. **DOI:** 10.1016/j.vacuum.2010.12.002
12. Schuchardt, A.; Braniste, T.; Mishra, Y. K.; Deng, M.; Mecklenburg, M.; Stevens-Kalceff, M. A.; Raevschi, S.; Schulte, K.; Kienle, L.; Adelung, R.; Tiginyanu, I.; *Scientific Reports 5*, **2015**, Article number: 8839. **DOI:** 10.1038/srep08839
13. Uchiyama, H.; Yukizawa, M.; Kozuka, H.; *J. Phys. Chem. C*, **2011**, *115*, 7050. **DOI:** 10.1021/jp112279k
14. Wang, Y.; Xu, J.; Wu, H; Xu, M; Peng, Z.; Zheng, G.; *J. Mater. Chem.*, **2012**, *22*, 21923. **DOI:** 10.1039/C2JM35255A
15. Tong, M. S.; Dai, G. R.; Gao, D. S.; *Vacuum*, **2000**, *59*, 877.
16. Kaur, G.; Mitra, A.; Yadav, K.L.; Adv. Mater. Lett., 2015, 6, 73. **DOI:** 10.5185/amlett.2015.5606
17. Chrisey, D. B. and Hubler, G. K.; Wiley: New York **1994**.
18. Sefardjella, H.; Boudjema, B.; Kabir, A.; Schmerber, G.; *Current Applied Physics*, **2013**, *13*, 1971. **DOI:** 10.1016/j.cap.2013.08.017
19. Bansal, S.; Pandya, D. K.; Kashyap, S. C.; Haranath, D.; *J. Alloys Compd.*, **2014**, *583*, 186. **DOI:** 10.1016/j.jallcom.2013.08.135
20. Muying, W; Shihui, Yu; Lin, He; Geng, Z; Dongxiong, L; Weifeng, Z.; *Appl. Surf. Sci.*, **2014**, *292*, 219. **DOI:** 10.1016/j.apsusc.2013.11.119
21. Korber, C.; Suffner, J.; Klein, A.; *J. Phys. D: Appl. Phys.*, **2010**, *43*, 055301. **DOI:** 10.1088/0022-3727/43/5/055301
22. Som, S.; Dutta, S.; Kumar, Vijay; Kumar, Vinod; Swart, H.C.; Sharma, S.K.; *J. Lumin.*, **2014**, *146*, 162. **DOI:** 10.1016/j.jlumin.2013.09.058
23. Balakrishnan G, Bandi, V. R; Rajeswari, S. M.; Balamurugan, N.; Babu, R.V.; Song, J. I.; *Mater. Res. Bull.*, **2013**, *48*, 4901. **DOI:** 10.1016/j.materresbull.2013.07.009
24. Kumar, Vinod; Som, S.; Kumar, Vijay; Ntwaeaborwa, O.M.; Coetsee, E.; Swart, H.C.; *Chem. Eng. J.*, **2014**, *255*, 541. **DOI:** 10.1016/j.cej.2014.06.027
25. Kilic, C; Zunger, A; *Phys. Rev. Lett.*, **2002**, *88*, 095501.
26. Kumar, Vinod; Kumar, Vijay; Som, S; Neethling, J. H.; Lee, Mike; Ntwaeaborwa, O. M. and Swart, H. C.; *Nanotechnology*, **2014**, *25*, 135701. **DOI:** 10.1088/0957-4484/25/13/135701
27. Som, S.; Kunti, A. K.; Kumar, Vinod; Kumar, Vijay; Dutta, S.; Chowdhury, M.; Sharma, S. K.; Terblans, J. J.; Swart, H. C.; *J. Appl. Phys*, 2014, 115, 193101. **DOI:** 10.1063/1.4876316
28. McCamy; C. S.; *Colour Res Appl.*, **1992**, *17*, 142.
29. Reddy, Y. A. K.; Reddy, A. S.; Reddy, P. S.; *J. Alloys Compd.*, **2014**, *583*, 396. **DOI:** 10.1016/j.jallcom.2013.08.180
30. Lee, J.; *Thin Solid Films*, **2008**, *516*, 1386. **DOI:**10.1016/j.tsf.2007.05.027
31. Lee, G.-H.; Ceramics International, 2015, 41, 12058 **DOI:**10.1016/j.ceramint.2015.06.021
32. Alaf, M.; Guler, M. O.; Gultekin, D.; Uysal, M.; Alp, A.; Akbulut, H.; *Vacuum*, **2009**, *83*, 292. **DOI:**10.1016/j.vacuum.2008.06.007
33. Chan y Diaz, E.; Camacho, Juan M.; Duarte-Moller, A.; Castro-Rodríguez, R.; Bartolo-Perez, P.; *J. Alloys Compd.*, **2010**, *508*, 342. **DOI:**10.1016/j.jallcom.2010.08.076